

Antiproton and Positron Signal Enhancement in Dark Matter Mini-Spikes Scenarios

Pierre Brun,^{1,*} Gianfranco Bertone,^{2,3,†} Julien Lavalle,^{4,‡} Pierre Salati,^{5,§} and Richard Taillet^{5,¶}

¹Laboratoire d'Annecy-le-Vieux de Physique des Particules LAPP,
Université de Savoie, CNRS/IN2P3, 74941 Annecy-le-vieux, France

²INFN, Sezione di Padova, Via Marzolo 8, Padova I-35131, Italy

³Institut d'Astrophysique de Paris, UMR 7095-CNRS,
Université Pierre et Marie Curie, 75014 Paris, France

⁴Centre de Physique des Particules de Marseille CPPM,
Université de la Méditerranée, CNRS/IN2P3, 13288 Marseille, France

⁵Laboratoire d'Annecy-le-Vieux de Physique Théorique LAPTH,
Université de Savoie, CNRS/IN2P3, 74941 Annecy-le-vieux, France

(Dated: September 14, 2021)

The annihilation of dark matter (DM) in the Galaxy could produce specific imprints on the spectra of antimatter species in Galactic cosmic rays, which could be detected by upcoming experiments such as PAMELA and AMS02. Recent studies show that the presence of substructures can enhance the annihilation signal by a "boost factor" that not only depends on energy, but that is intrinsically a statistical property of the distribution of DM substructures inside the Milky Way. We investigate a scenario in which substructures consist of ~ 100 "mini-spikes" around intermediate-mass black holes. Focusing on primary positrons and antiprotons, we find large boost factors, up to a few thousand, that exhibit a large variance at high energy in the case of positrons and at low energy in the case of antiprotons. As a consequence, an estimate of the DM particle mass based on the observed cut-off in the positron spectrum could lead to a substantial underestimate of its actual value.

PACS numbers:

LAPP-EXP-2007-02, LAPTH-1181/07, CPPM-P-2007-01

Many current and upcoming experiments are aimed at detecting the products of annihilation of dark matter particles in the Milky Way halo, or in external galaxies – see Refs. [1, 2, 3] for recent reviews. In fact, the identification of an annihilation signal would not only provide the proof of the particle nature of DM, but it would also open a new window to Physics beyond the Standard Model. Among indirect searches, particular attention has been devoted to the case of photons, since they propagate along straight lines, and they are not significantly absorbed within the galaxy at energies of order 100 GeV and below. The prospects for detecting gamma-rays from DM annihilation with the space telescope GLAST [4] and with Air Cherenkov telescopes such as CANGAROO [5], HESS [6], MAGIC [7] and VERITAS [8], have been extensively discussed in literature – e.g. [52] and references therein. Alternatively, one may search for neutrino fluxes from DM captured at the center of the Sun or of the Earth – see reviews above for further details – with large neutrino telescopes such as IceCube [9] and Antares [10].

One can also focus on other final states of DM annihilation, such as antimatter particles, in particular positrons [11, 12, 13, 14, 15, 16, 17, 18, 19] and antiprotons [20, 21, 22, 23]. Unlike photons and neutrinos, these

are charged particles that are sensitive to the galactic magnetic field and suffer energy losses. Their propagation must be described by diffusion, so that the magnetic properties of the Milky Way must be known, which is not completely true yet. Nevertheless, it is possible to make interesting predictions, which are now particularly relevant, as the recently launched satellite PAMELA [24] and the forthcoming AMS02 [25] experiment are expected to provide new data and test a significant portion of the parameter space of DM particles.

In most cases, the prospects for the detection of antimatter fluxes are not particularly sensitive to the overall shape of the DM profile, but they do depend strongly on the "clumpiness" of the profile. In fact, the annihilation rate being proportional to the square of the number density, the presence of small-scale inhomogeneities leads to larger fluxes for the same value of the average DM density. This is often parameterized by a "boost factor", that will be defined more precisely below.

Recently, a new scenario has been discussed in the literature, where the formation of Intermediate Mass Black Holes, i.e. Black Holes with mass M in the range $10^2 \lesssim M/M_\odot \lesssim 10^6$, leads to the formation of DM overdensities, called "mini-spikes", that might be observed as point sources of gamma-rays [40] and neutrinos [26]. Although somewhat speculative, the scenario has the undisputed virtue of making specific predictions on the number and luminosity of these objects, that could be observed or ruled out in the near future with the upcoming generation of space and ground based experiments. Here, we compute the boost factor in mini-spikes scenarios, and argue that they would lead to a dramatic enhancement

*Electronic address: brun@lapp.in2p3.fr

†Electronic address: bertone@iap.fr

‡Electronic address: lavalle@in2p3.fr

§Electronic address: salati@lapp.in2p3.fr

¶Electronic address: taillet@lapp.in2p3.fr

of antimatter fluxes, bringing them within the reach of current and upcoming experiments.

The paper is organized as follows : in Section **I**, we review the motivations for the mini-spike scenario and derive their density profile and normalization. Section **II** is devoted to a general discussion of the antimatter cosmic ray signal generated by mini-spikes. The average value and the variance of the boost factor at the Earth are defined and special attention is paid to the inner structure and galactic distribution of the mini-spikes. Positrons and antiprotons are respectively addressed in Sections **III** and **IV**. Results from Monte-Carlo simulations are presented and discussed in the light of analytic calculations. The energy dependence of the boost variance turns out to be quite different for positrons and antiprotons. These species have very different modes of propagation inside the Milky Way. A few realistic models for the DM particles are implemented in Section **V**. The positron and antiproton signals which they yield are featured and illustrate the typical antimatter signatures to be expected should mini-spikes populate the galactic halo. We finally conclude in Section **VI** and make a few suggestions for future developments.

I. MINI-SPIKES AS DM SUBSTRUCTURES

Black Holes (BHs) can be broadly divided in three different classes – see e.g. [27] for a review :

- *Stellar Mass BHs*, with mass $M \lesssim 100 M_{\odot}$. They are typically remnants of the collapse of massive stars. Recent simulations suggest that the upper limit on the mass of these objects is as low as $\approx 20 M_{\odot}$ [28]. There is *robust* evidence for the existence of these objects, coming from the observation of binary systems with compact members whose mass exceeds the critical mass of Neutron Stars. For a review of the topic and the discussion of the status of the observational evidence for Stellar Mass BHs see e.g. [29] and references therein.
- *Supermassive BHs (SMBHs)*, with mass $M \gtrsim 10^6 M_{\odot}$ lying at the centers of galaxies, including our own. Their existence is also well-established – see e.g. Ref. [30] – and intriguing correlations are observed between the SMBHs mass and the properties of their host galaxies and halos [31, 32, 33, 34, 35, 45]. From a theoretical point of view, a population of massive seed black holes could help to explain the origin of SMBHs. In fact, observations of quasars at redshift $z \approx 6$ in the Sloan Digital survey [36, 37, 38] suggest that SMBHs were already in place when the Universe was only ~ 1 Gyr old, a circumstance that can be understood in terms of a rapid growth starting from “massive” seeds – see e.g. Ref. [39]. This leads to the third category:
- *Intermediate Mass BHs (IMBHs)*, with mass $10^2 \lesssim M/M_{\odot} \lesssim 10^6$. Scenarios that seek to explain

the properties of the observed supermassive black holes population result in the prediction of a large population of wandering Intermediate Mass BHs (IMBHs). Here, following Ref. [40], we consider two different formation scenarios for IMBHs. In the first scheme (A), IMBHs form in rare, overdense regions at high redshift, $z \sim 20$, as remnants of Population III stars, and have a characteristic mass-scale of a few $10^2 M_{\odot}$ [41] – a similar model was investigated in Ref. [42, 43, 44]. In this scenario, these black holes serve as the seeds for the growth of supermassive black holes found in galactic spheroids [30]. In the second scenario (B), IMBHs form directly out of cold gas in early-forming halos and are typified by a larger mass scale of order $10^5 M_{\odot}$ [45]. During the virialization and collapse of the first halos, gas cools, collapses, and forms pressure-supported disks at the centers of halos that are massive enough to contain a large amount of molecular hydrogen. In halos which do not experience any major mergers over a dynamical time, a protogalactic disk forms and can evolve uninterrupted. At this stage, an effective viscosity due to local gravitational instabilities in the disk leads to an inward mass transfer and outward angular momentum transfer, until supernovae in the first generation of stars heat the disk and terminate this process. By the time the process terminates, a baryonic mass of order $\sim 10^5 M_{\odot}$ loses its angular momentum and is transferred to the center of the halo, leading to the formation of an object that may be briefly pressure-supported, but that eventually collapses to form a black hole. In Fig. 4 we show the distribution of IMBHs in the latter scenario, as obtained in Ref. [26].

The effect of the formation of a central object on the surrounding distribution of matter has been investigated in Refs. [46, 47, 48, 49] and for the first time in the framework of DM annihilations in Ref. [50]. It was shown that the *adiabatic* growth of a massive object at the center of a power-law distribution of DM, with index γ , induces a redistribution of matter into a new power-law (dubbed “spike”) with index

$$\gamma_{\text{sp}} = (9 - 2\gamma)/(4 - \gamma) . \quad (1)$$

This formula is valid over a region of size $R_{\text{sp}} \approx 0.2 r_{\text{BH}}$, where r_{BH} is the radius of gravitational influence of the black hole, defined implicitly as $M(< r_{\text{BH}}) = M_{\text{BH}}$, where $M(< r)$ denotes the mass of the DM distribution within a sphere of radius r , and where M_{BH} is the mass of the Black Hole [51]. The process of adiabatic growth is in particular valid for the SMBH at the galactic center. A critical assessment of the formation *and survival* of the central spike, over cosmological timescales, is presented in Refs. [52, 53] – see also references therein. Adiabatic spikes are rather fragile structures, that require fine-tuned conditions to form at the center of galactic

halos [54], and that can be easily destroyed by dynamical processes such as major mergers [55] and gravitational scattering off stars [53, 56].

It was recently shown that a $\rho \propto r^{-3/2}$ DM overdensity can be predicted in any halo at the center of any galaxy old enough to have grown a power-law density cusp *in the stars* via the Bahcall-Wolf mechanism [57]. Collisional generation of these DM “crests” – Collisionally REgenerated STructures – was demonstrated even in the extreme case where the DM density was lowered by slingshot ejection from a binary supermassive black hole. However, the enhancement of the annihilation signal from a DM crest is typically much smaller than for adiabatic spikes [57].

Here we focus our attention on *mini-spikes* around IMBHs, and we recall their properties, following closely Ref. [40]. The “initial” DM mini-halo – that is, the DM distribution prior to black hole formation – can be well approximated with a Navarro, Frenk, and White (NFW) profile [58]

$$\rho(r) = \rho_0 \left(\frac{r}{r_{\text{sc}}} \right)^{-1} \left(1 + \frac{r}{r_{\text{sc}}} \right)^{-2} . \quad (2)$$

The normalization constant ρ_0 , and the scale radius r_{sc} , can be expressed in terms of the virial mass M_{vir} of the halo at the time when the IMBH formed, and of the virial concentration parameter c_{vir} – see Ref. [40] for further details. Alternatively, we could have chosen the more recent parameterization proposed by Navarro et al. [59] – see also Refs. [60, 61]. However, this profile implies modifications at scales smaller than those we are interested in, where the profile is anyway modified by the presence of the IMBH. We assume that the black holes form over a timescale long enough to guarantee adiabaticity, but short compared to the cosmological evolution of the host halo. In fact, the condition of “adiabaticity”, fundamental to grow mini-spikes, requires that the formation time of the black hole is much larger than the dynamical timescale at a distance r_{BH} from the black hole, where $r_{\text{BH}} \simeq GM_{\text{BH}}/\sigma^2$ is the radius of the sphere of gravitational influence of the black hole, and σ is the velocity dispersion of DM particles at r_{BH} . In practice, r_{BH} is estimated by solving the implicit equation

$$M(< r_{\text{BH}}) \equiv \int_0^{r_{\text{BH}}} \rho_{\text{tot}}(r) 4\pi r^2 dr = 2 M_{\text{BH}} . \quad (3)$$

In the following, we only consider the formation scenario B, which leads to higher values for the boost factor. For a representative case in scenario B, with $M_{\text{BH}} = 10^5 M_{\odot}$ and $M_{\text{vir},f} = 10^8 M_{\odot}$, this gives $r_{\text{BH}}/r_{\text{sc}} \approx 0.04$. In scenario B, the black hole formation time is set by the timescale for viscous angular momentum loss and is limited by the evolutionary timescale of the first stars and the gravitational infall time across the gaseous disk, which is of order Myr – see Ref. [62] for a detailed discussion of timescales. The relevant timescale for the mass build up of the IMBH is then $t_{\text{ev}} \sim 1 - 20$ Myr.

II. THE ANTIMATTER COSMIC RAY SIGNAL PRODUCED BY MINI-SPIKES

A. Fluxes at the Earth

The self-annihilations of the DM particles χ concealed in the Milky Way halo produce positrons and antiprotons, a small fraction of which may reach the Earth. The local production rate of these antimatter cosmic ray species will be generically denoted by

$$\mathcal{P}(\mathbf{x}) = \delta \langle \sigma_{\text{ann}} v \rangle \left\{ \frac{\rho_{\chi}(\mathbf{x})}{m_{\chi}} \right\}^2 g(E_S) \Delta E_S . \quad (4)$$

The factor δ is equal to 1/2 if the DM particles χ are Majorana fermions whereas it is 1/4 in the case of Dirac species, provided that a perfect matter-antimatter symmetry between χ and $\bar{\chi}$ holds in that case. Until Section V, we will focus our discussion on monoenergetic positrons and antiprotons with energy E_S defined up to an energy bandwidth of ΔE_S . In Kaluza-Klein theories of dark matter particles, the branching ratio into an e^+e^- pair can be as large as $B_{e^{\pm}} \sim 20\%$ [63] and the energy distribution $g(E_S)$ of Eq. (4) is equal to $B_{e^{\pm}} \delta(E_S - m_{\chi})$, where m_{χ} stands for the mass of the DM species. In the case of antiprotons, energy losses may be neglected and we need only to consider a specific value of the initial energy E_S . A continuous injection spectrum will be considered in Section V, as is needed for realistic models of antimatter production.

The probability for a cosmic ray species injected at \mathbf{x} to propagate and reach the Earth with energy E is described by the Green function

$$G(\mathbf{x}) \equiv G(E, \odot \leftarrow E_S, \mathbf{x}) . \quad (5)$$

The propagator $G(\mathbf{x})$ has been thoroughly discussed in the literature – see Refs. [16, 19] for positrons and Refs. [64, 65] for antiprotons. The annihilations of DM particles yield the following flux at the Earth

$$\phi(E) = \mathcal{S} \int_{\text{DM halo}} G(\mathbf{x}) \left\{ \frac{\rho_{\chi}(\mathbf{x})}{\rho_0} \right\}^2 d^3\mathbf{x} , \quad (6)$$

which is expressed in units of $\text{cm}^{-2} \text{s}^{-1} \text{sr}^{-1} \text{GeV}^{-1}$. The factor \mathcal{S} encodes informations on the specific model selected to describe the DM species χ such as its mass m_{χ} and total annihilation cross section $\langle \sigma_{\text{ann}} v \rangle$. It is defined as

$$\mathcal{S} = \frac{\delta}{4\pi} \beta(E) \langle \sigma_{\text{ann}} v \rangle \left\{ \frac{\rho_0}{m_{\chi}} \right\}^2 g(E_S) \Delta E_S . \quad (7)$$

The velocity of the cosmic ray particles is denoted by $\beta(E)$ and ρ_0 is a reference density that can be chosen at will, eventually disappearing from the final result. It can be given a physical meaning, as we will see when we define the annihilation volume ξ .

B. The framework of the statistical analysis

In the absence of any substructure, the DM distribution ρ_s is smooth and yields a cosmic ray flux

$$\phi_s(E) = \mathcal{S} \int_{\text{DM halo}} G(\mathbf{x}) \left\{ \frac{\rho_s(\mathbf{x})}{\rho_0} \right\}^2 d^3\mathbf{x} . \quad (8)$$

In the IMBHs scenario, the DM distribution is given by the superposition $\rho = \rho_s + \delta\rho$ where a new component $\delta\rho \gg \rho_s$ accounts now for the DM trapped inside the mini-spikes. That component contributes for a fraction of $\sim 10^{-5}$ to the Galactic dark matter. As the typical distance over which positrons and antiprotons propagate in the Milky Way is much larger than the average size of the mini-spikes, the cosmic ray flux – generated by the total density ρ – simplifies into the sum

$$\phi(E) = \phi_s + \left(\phi_r = \sum_i \varphi_i \right) , \quad (9)$$

where the contribution from the i -th object is $\varphi_i = \mathcal{S} \times G(\mathbf{x}_i) \times \xi_i$. That substructure produces as many positrons and antiprotons as if the entire volume

$$\xi_i = \int_{i\text{-th mini-spike}} \left\{ \frac{\delta\rho(\mathbf{x})}{\rho_0} \right\}^2 d^3\mathbf{x} \quad (10)$$

were filled with the constant DM density ρ_0 . The mini-spike mass M_i and *intrinsic* boost B_i are related to the annihilation volume ξ_i through

$$\xi_i \equiv \frac{B_i M_i}{\rho_0} . \quad (11)$$

Note that the exotic flux φ_i has no well-defined dependence on the mass M_i and the intrinsic boost B_i if these quantities are considered individually, since φ_i only depends on the annihilation volume ξ_i .

Should we know the exact location and annihilation volume of each mini-spike, we would unambiguously derive the cosmic ray flux $\phi(E)$. This is not the case, and for that matter we do not even know the number N_{BH} of these objects. Very different distributions of the mini-spike population throughout the galactic halo are possible. The positron and antiproton spectra at the Earth are therefore affected by an uncertainty (which could be called a cosmic variance) related to this lack of knowledge. A whole set of halo realizations has to be considered, and specific semi-analytical tools have been developed [19] to address this issue. The boost factor $B = \phi/\phi_s$ at the Earth is not unique and must be treated as a random variable. To do so, we have built a Monte-Carlo simulation nurtured by ~ 200 different realizations of the mini-spike population which have been obtained in Ref. [40] by evolving an initial distribution of IMBHs orbiting in the Milky Way halo and by allowing the associated DM mini-halos to be tidally destroyed

during close encounters. The distribution of the number N_{BH} of surviving mini-spikes is presented in Fig. 1. In our Monte-Carlo simulation, N_{BH} is randomly drawn according to a gaussian distribution. About 100 objects are expected within a 100 kpc galactocentric radius and ~ 60 of them populate the Galactic diffusive halo.

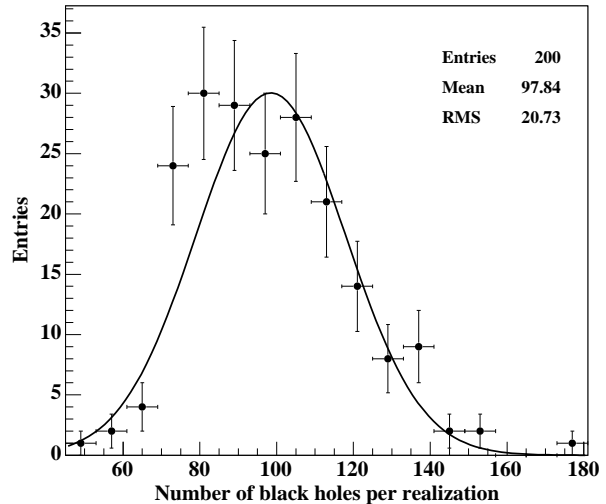


FIG. 1: Distribution of the Monte-Carlo realizations of the galactic mini-spike population – extracted from Ref. [40] – as a function of the number N_{BH} of objects within a galactocentric radius of 100 kpc.

If we set N_{BH} equal to its mean value, we may derive analytically the average value and the variance of the boost factor B according to the method presented in Ref. [19]. We did not find any significant correlation between the position \mathbf{x} and annihilation volume ξ of the mini-spikes in the simulations of Ref. [40], so that they seem to be distributed independently of the others. We readily infer an average boost factor of

$$B_{\text{eff}} = 1 + \frac{\langle \phi_r \rangle}{\phi_s} = 1 + N_{\text{BH}} \frac{\langle \xi \rangle \langle G \rangle}{\mathcal{I}} . \quad (12)$$

The integral \mathcal{I} stands for the convolution of the propagator G with the smooth DM distribution ρ_s

$$\mathcal{I} = \int_{\text{DM halo}} G(\mathbf{x}) \left\{ \frac{\rho_s(\mathbf{x})}{\rho_0} \right\}^2 d^3\mathbf{x} , \quad (13)$$

In the following, a NFW profile is assumed, where a value $\rho_{\odot} = 0.3 \text{ GeV/cm}^3$ is considered for the Solar dark matter density. The mini-spike annihilation volume and galactic position are respectively distributed according to the probability functions $q(\xi)$ and $p(\mathbf{x})$ which are presented in Sections II C and II D. These probability laws allow to define the average values

$$\langle G^n \rangle = \int_{\text{DM halo}} \{G(\mathbf{x})\}^n p(\mathbf{x}) d^3\mathbf{x} , \quad (14)$$

and

$$\langle \xi^n \rangle = \int_0^{+\infty} \xi^n q(\xi) d\xi . \quad (15)$$

In practice, we will only be concerned with $n = 1$ and 2. The boost scatter σ_B may be derived from the relation

$$\frac{\sigma_B}{B_{\text{eff}}} = \frac{\sigma_r / \phi_s}{1 + \langle \phi_r \rangle / \phi_s} \simeq \frac{\sigma_r}{\langle \phi_r \rangle} , \quad (16)$$

where the variance σ_r of the random flux component ϕ_r is given by

$$\frac{\sigma_r^2}{\langle \phi_r \rangle^2} = \frac{1}{\langle N_{\text{BH}} \rangle} \left(\frac{\sigma_\xi^2}{\langle \xi \rangle^2} + \frac{\sigma_G^2}{\langle G \rangle^2} + \frac{\sigma_\xi^2 \sigma_G^2}{\langle \xi \rangle^2 \langle G \rangle^2} \right) + \frac{\sigma_N^2}{\langle N_{\text{BH}} \rangle^2} , \quad (17)$$

where σ_ξ , σ_G and σ_N stand for the variances of the respective distributions. In Sections III and IV, we will check the consistency of our Monte-Carlo results in the light of the analytic expressions (12) and (16).

C. The inner structure of mini-spikes

In the case where the DM profile *before* the formation of the IMBH follows the commonly adopted NFW distribution [58], the final DM density $\rho(r)$ around the IMBH will be described by a power law $r^{-7/3}$ in a region of size R_{sp} .

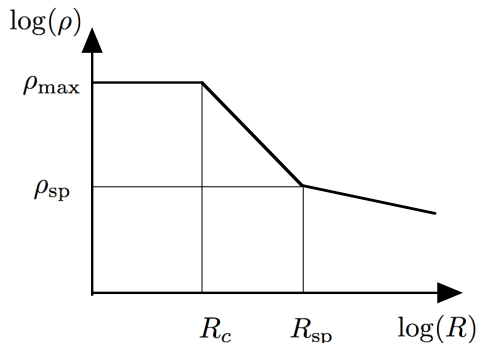


FIG. 2: Schematic representation of the inner structure of a mini-spike

At larger distances, the DM distribution has not been modified by the accretion onto the IMBH and the density still falls down as r^{-1} . This envelope does not contribute significantly to the DM annihilation and its associated production of positrons and antiprotons. On the contrary, the DM density steeply increases below R_{sp} and annihilations themselves set an upper limit to it

$$\rho_{\text{max}} \approx \frac{m_\chi}{\langle \sigma_{\text{ann}} v \rangle \tau} , \quad (18)$$

where τ is the time elapsed since the formation of the mini-spike. We denote by R_c the “cut-off” radius below which the mini-spike core extends with uniform density ρ_{max} . For a typical value of $\tau = 10$ Gyr, we find

$$\rho_{\text{max}} = 8.752 \times 10^{15} \times \left(\frac{m_\chi}{\text{GeV}} \right) \times \left(\frac{\langle \sigma_{\text{ann}} v \rangle}{10^{-26} \text{ cm}^3 \text{ s}^{-1}} \right)^{-1} M_\odot \text{ kpc}^{-3} . \quad (19)$$

The relative extension of the mini-spike mantle ($R_c \leq r \leq R_{\text{sp}}$) with respect to the core ($r \leq R_c$) is given by

$$\frac{R_{\text{sp}}}{R_c} = \left\{ \eta \equiv \frac{\rho_{\text{max}}}{\rho_{\text{sp}}} \right\}^{3/7} , \quad (20)$$

where $\rho_{\text{sp}} = \rho(R_{\text{sp}})$ is the DM density at the surface $r = R_{\text{sp}}$ of the mantle. Integrating Eq. (10) over the inner structure of the mini-spike leads to the annihilation volume

$$\xi = \frac{12}{5} \pi R_{\text{sp}}^3 \left\{ \frac{\rho_{\text{sp}}}{\rho_0} \right\}^2 \left\{ \frac{14}{9} \eta^{5/7} - 1 \right\} . \quad (21)$$

Due to the different mini-spike features (much less steep DM profile), the case of scenario A leads to much lower annihilation volumes. This case is no more mentioned in the following.

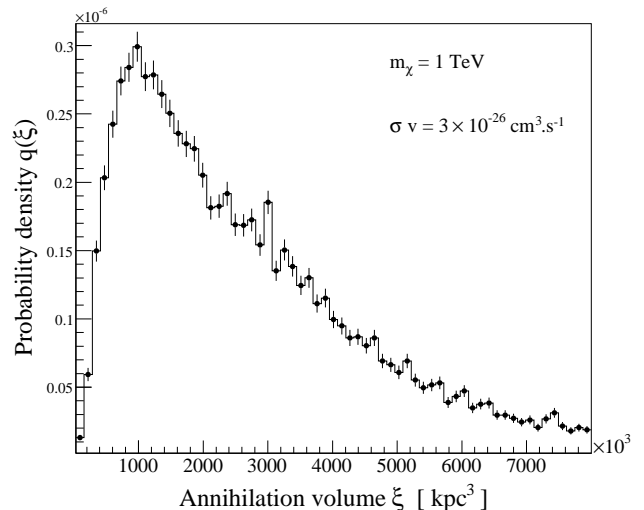


FIG. 3: The probability law $q(\xi)$ for the annihilation volume has been derived from the Monte-Carlo results of Ref. [40]. We found no correlation with the mini-spike position.

We have derived the probability function for ξ from the Monte-Carlo results of Ref. [40] where the mini-spike radius R_{sp} and external density ρ_{sp} are provided for each object. This distribution – featured in Fig. 3 – is characterized by very large values of the annihilation volume, with a tail extending up to $\xi \sim 1.2 \times 10^7 \text{ kpc}^3$. On average, with a mini-spike radius $R_{\text{sp}} = 2.84 \text{ pc}$ and density

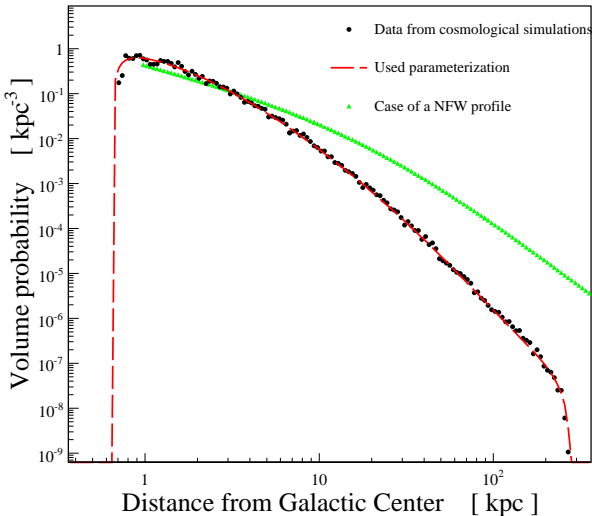


FIG. 4: Radial distribution of the mini-spikes, as extracted from the numerical results of Ref. [40].

$\rho_{\text{sp}} = 48.51 \text{ M}_{\odot} \text{ pc}^{-3}$, we infer a typical annihilation volume $\xi \sim 3.3 \times 10^6 \text{ kpc}^3$ for a benchmark cross section $\langle \sigma_{\text{ann}} v \rangle = 3 \times 10^{-26} \text{ cm}^3 \text{ s}^{-1}$, a mass $m_{\chi} = 1 \text{ TeV}$ and $\rho_0 \equiv \rho_{\odot} = 0.3 \text{ GeV cm}^{-3}$. The distribution of ξ happens to be log-normal. In our Monte-Carlo program, we simulate a large number of different IMBH halo populations. For each mini-spike, the annihilation volume ξ is randomly chosen according to the $q(\xi)$ distribution.

Notice finally that the individual mini-spike contribution φ_i scales as the product $\mathcal{S} \times \xi_i$ and is eventually proportional to

$$\varphi_{\text{mini-spike}} \propto \langle \sigma_{\text{ann}} v \rangle^{2/7} m_{\chi}^{-9/7}. \quad (22)$$

The cosmic ray signal depends weakly on the annihilation cross section since a decrease of the cross section is partially compensated by a higher annihilation volume. This issue is addressed with more details in Section V, where the influence of the injection spectrum $g(E_S)$ will also be considered.

D. The galactic distribution of mini-spikes

The Monte-Carlo simulation of IMBHs formation and evolution is used to derive the distribution function $p(r)$ for the galactocentric radius of each mini-spike that has survived tidal disruption. This function gives the probability to find an object at galactocentric distance r within a spherical shell of thickness dr . It is expressed in units of kpc^{-3} and normalized to unity within the inner 100 kpc. This volume distribution is presented in Fig. 4 together with the parameterized function used in the following to estimate the boost factors.

The mini-spike number density drops quickly beyond a few hundred parsecs from the galactic center. This is

because encounters and mergers are much more frequent in this region, and they are very efficient in disrupting dark matter spikes. For those which have survived, the logarithmic slope of the radial profile varies from ~ 1.8 in the inner region to ~ 3.8 outward. This distribution is more peaked than for a typical NFW profile whose corresponding volume probability is also drawn in Fig. 4 for comparison.

III. RESULTS FOR POSITRONS

This section is devoted to the positron signal. For pedagogical purposes, we first consider a fiducial case in which dark matter consists in $m_{\chi} = 1 \text{ TeV}$ particles fully annihilating at rest in electron-positron lines. In this very simple frame, we scrutinize the positron flux enhancement that mini-spikes produce with respect to a single smooth distribution of dark matter in the Galaxy

The propagator for positrons is given by [19]. The energy at which a positron is detected on Earth depends on its propagation history. It is correlated to the distance over which it has diffused from the source. As a result, the flux at a given (detected) energy depends on the spatial distribution of the sources, i.e. on clumpiness. In this section, we study this effect in a more quantitative way.

A. The Monte-Carlo simulation

We have performed Monte-Carlo simulations of the mini-spike spatial distribution in the halo. Each halo configuration yielded a value for the positron flux $\phi_r = \sum \varphi_i$, from which the average boost factor and the corresponding variance could be computed. The probability density functions for the number N_{BH} of IMBHs, their position \mathbf{x}_i and annihilation volume ξ_i were based on cosmological simulations from Ref. [40]. The corresponding probability laws have been presented in Section II. The propagated flux is compared to the flux produced by a smooth NFW profile to determine the boost factor.

B. The numerical results

Monte-Carlo simulations involving 10^6 realizations of the IMBHs population have been performed. The mean value and the variance of the resulting boost factors (for positron flux) at the Earth is sketched in Fig. 5 as a function of energy. The shaded area show the region where the boost factor is expected to lie, with a $1\text{-}\sigma$ and $2\text{-}\sigma$ confidence level.

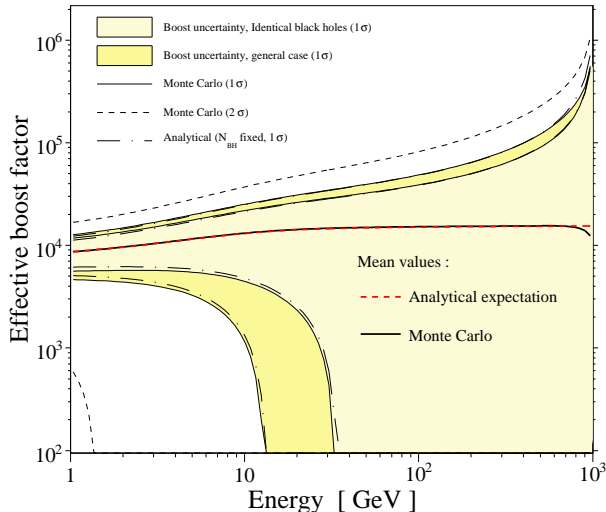


FIG. 5: Results from the Monte-Carlo simulations of the IMBHs population inside the Milky Way are compared to the analytical computations of the effective boost factor and its dispersion, for $m_\chi = 1$ TeV.

The yellow (grey) areas correspond to the 1σ region, the lighter one being obtained by fixing the annihilation volumes ξ_i to their mean expected value, while the darker one corresponds to the general case for which mini-spikes have values of ξ_i drawn according to their true probability distribution $q(\xi)$. In both cases, the dot-dashed curves stand for the 1σ contours obtained analytically. These curves are in good agreement with the ones obtained from the Monte Carlo, the small increase of the variance for the Monte Carlo with respect to the analytical expectation is due to the variation of the black holes number from one Monte Carlo realization to another, while this effect is not implemented in the analytical determination of the boost factor. The fact that these curves are fairly close to each other confirms that the dispersion of the number N_{BH} of IMBHs in the Milky Way poorly influences the final dispersion of the boost. This figure also shows that the boost factor can be very large, the expected value being of order 8000 (for a DM particle mass of 1 TeV).

Fig. 5 shows that the variance increases with energy, and becomes very large for $E \gtrsim 20$ GeV. It clearly appears that the boost factor obeys two different statistical regimes. This is because the diffusive range of positrons depends on energy and a positron emitted with energy E_s loses energy as it propagates outwards from the source. The typical propagation scale for a positron injected with energy E_s and detected with energy E is given by

$$\lambda_D \equiv \sqrt{4K_0\tau_E (\epsilon^{\delta-1} - \epsilon_S^{\delta-1}) / (1-\delta)}, \quad (23)$$

where K_0 and δ are respectively the normalization and the logarithmic slope of the diffusion coefficient, and $\epsilon \equiv (E/1 \text{ GeV})$. We have considered the median parameters given in [21], $K_0 = 0.0112 \text{ kpc}^2 \text{ Gyr}^{-1}$, $L = 4 \text{ kpc}$,

$V_c = 12 \text{ km/s}$ and $\delta = 0.7$. The typical timescale for energy loss of 1 GeV positrons is $\tau_E \approx 10^{16} \text{ s}$. For a 1 TeV injected energy, we infer a propagation length $\lambda_D \approx 6.9 \text{ kpc} \times \sqrt{\epsilon^{-0.3} - 0.12}$, which ranges from 0.1 kpc at a detected energy of 990 GeV to 6.4 kpc at 1 GeV.

At high energy, this diffusive range is very short, and positrons will be detected only provided there happens to be a mini-spike very close to us. The probability of this event is low at energy close to E_s , but the contribution to the flux is high if it happens. The trade-off between these two trends leads to a constant expectation value for the boost factor, but a large shotnoise-like variance. Conversely, at low energy the diffusive range is large, and the fluctuations in the number of sources contributing to the flux becomes relatively small.

The distributions of the boost factor at 1 GeV obtained with Monte Carlo simulations are displayed in the left panel of Fig. 6. The red histogram corresponds to the case of identical mini-spikes with fixed annihilation volume. It can be compared to the analytical estimate of the boost factor distribution (dashed curve) in the limiting case where the number of IMBHs is large enough for the central-limit theorem to be valid. If it were so, the distribution of the boost factor would tend to be gaussian. One can see that it is almost the case for identical objects. Though unrealistic, the case in which ten times more IMBHs populate the Milky Way leads actually to a gaussian distribution for $B(1 \text{ GeV})$ (not shown here). The statistics obtained in the general case is plotted in black, one can see that the effect of having different annihilation volumes for different mini-spikes shifts the distribution away from the gaussian behavior.

The right panel of Fig. 6 displays the distribution of the boost factor at 300 GeV. Again, the red histogram corresponds to the identical IMBHs case and should be compared to the analytical estimate (dashed curve). The latter includes only one IMBH inside the sensitivity volume so that the extra events of the red curve correspond to the (very) rare situations in which two mini-spikes contribute to the signal. This feature is not present in the general case, for which the statistics is displayed in black: it is erased by the random choice of ξ .

IV. RESULTS FOR ANTIPROTONS

A. Propagator

The propagator of antiprotons has a larger range than for positrons, and the effect of escape at the galactic boundaries must be considered. Modelling the galaxy as a cylinder of radius $R \sim 20 \text{ kpc}$ and of unknown height $2L$, in which antiprotons diffuse with an energy-dependent coefficient K , the solution of the diffusion equation can be obtained as Bessel-Fourier expansion over the r and z variables. It turns out that the side boundaries ($r = R$) can be neglected in most situations,

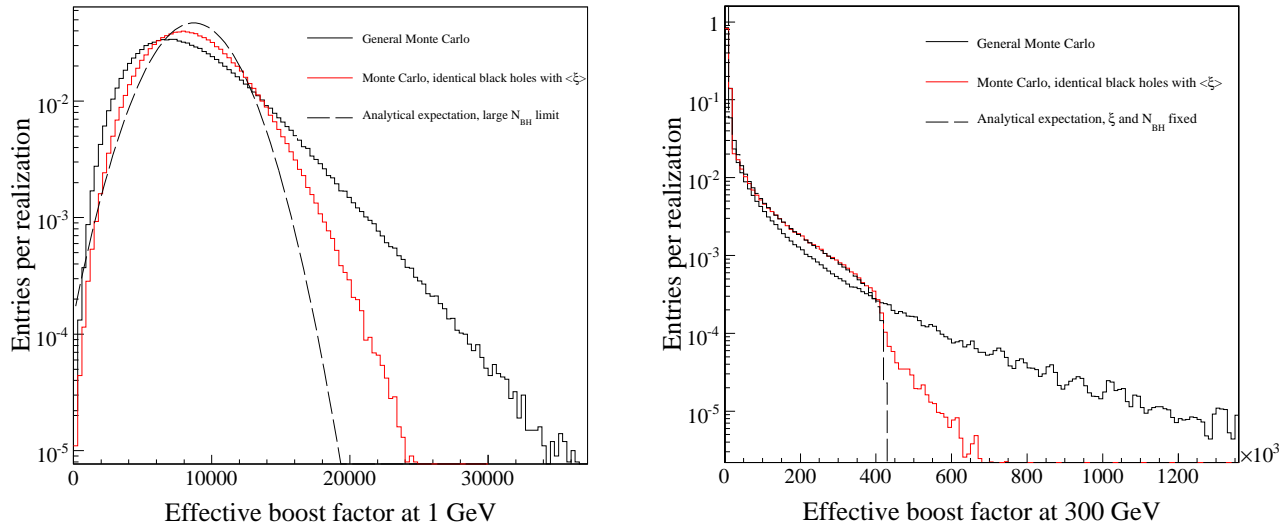


FIG. 6: Distribution of the boost factors at 1 GeV (left panel) and 300 GeV (right panel) obtained with the Monte Carlo simulations and comparison to analytical expectations (see text for further details). The gaussian distribution discussed in the text is plotted in the left panel (long-dashed curve).

as the $z = \pm L$ boundaries are closer to the solar neighborhood and influence more strongly the measured cosmic ray flux. As a consequence, the problem is essentially two-dimensional and the propagator from any source to the Earth can be expressed as a function of r and z only. Moreover, the sources (the mini-spikes) can be considered as point-like as far as the propagation over galactic distances is considered, and special care has to be taken for the singular $1/r$ dependence of $G(r, z)$. This point has been exposed in detail in [65], along with the corresponding analytical expressions for $G(r, z)$. The main difference with the positron case is that the energy losses due to radiative losses are much less important for antiprotons. If the diffusion is supposed to occur at constant energy, then the spatial distribution of antiprotons created in a given mini-spike is the same at every energy, and the boost factor should be energy-independent (see below). There are actually at least two effects that depend on energy, namely spallation and galactic wind. Their influence will be discussed below, along with the results. We have considered the same median parameters as in the positron case.

B. The Monte-Carlo simulation

Following the same method as for positrons, we have performed Monte-Carlo simulations of the IMBHs distribution, in order to estimate the expected antiproton flux, along with the associated variance. The procedure is exactly the same as before, and this section is devoted to the presentation of the results.

C. Expected values and variance of the boost factor

The average boost factor and its scatter are computed, both by direct evaluation of Eqs. (12) and (16) as well as by the Monte-Carlo simulation. Since energy losses are less important for antiprotons than for positrons, we find that when spallation and galactic wind are neglected, the boost factor does not depend on energy – see Fig. 7. When galactic wind is considered, propagation becomes energy-dependent at low energy, and so does the boost factor – see the dotted line in Fig. 7. The uncertainty band widens significantly below a few GeV. The importance of the galactic wind can be estimated through the Peclet number defined as $Pe \equiv V_c L / K$, the effect of the wind being negligible for small values of Pe . The diffusion coefficient K is a growing function of energy, so propagation is dominated by diffusion at high energy, whereas the wind has a sizeable effect at low energy. As the galactic wind is directed outward from the disk, it prevents antiprotons from reaching the Earth. As a result, the range of diffusion is lowered and the number of sources actually contributing to the signal is also lowered. This explains the large variance at low energy.

We see that the uncertainty on the antiproton flux is about one order of magnitude in the best case, i.e. with no energy-dependent processes. When both spallation and wind are considered, the prediction of the boost factor becomes meaningless below ~ 20 GeV. Notice however that when the thickness of the diffusive halo is larger, more mini-spikes contribute to the signal at the Earth and the variance decreases at all energies.

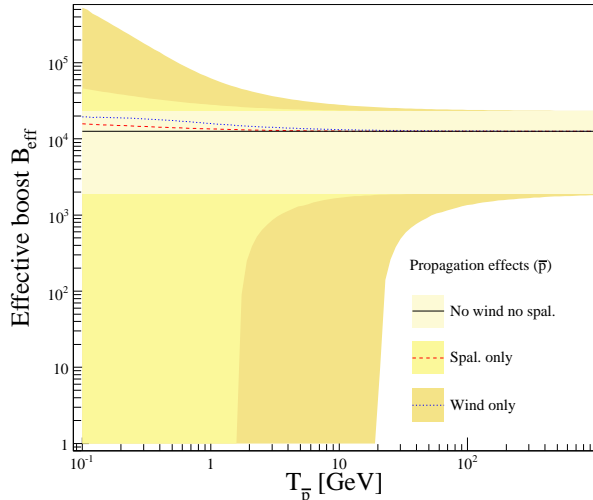


FIG. 7: Expected value and variance of the boost factor of the antiproton signal as a function of kinetic energy, in the case of a dark matter particle with mass $m_\chi = 1$ TeV and for different \bar{p} propagation configurations.

V. A FEW REALISTIC MODELS FOR THE DM PARTICLE

We have so far considered a generic case for the DM particle, with a mass of 1 TeV and a typical weak-scale annihilation cross section. This part is devoted to the estimate of the positron and antiproton exotic fluxes within specific particle physics models. We choose four typical DM particle candidates in the frameworks of supersymmetry and extra-dimensions.

All of these match the constraints from collider experiments and relic density. The smooth halo is modelled by a NFW profile with a Solar dark matter density $\rho_\odot = 0.3$ GeV/cm³. In the previous computations (positronic line, energy independent diffusion of antiprotons), the energy distribution at the source $g(E_S)$ was not relevant since it cancelled in the ratio ϕ_r/ϕ_s . In this section, we make predictions for the flux and we perform the convolution of the propagator with the injection spectrum $g(E_S)$. This is true in particular in the case of positrons, for which energy losses are more significant than for antiprotons. The injection spectrum depends on the final states of the DM particle annihilation process. In all the models we considered, these spectra have been computed with PYTHIA [67]. The annihilation cross section plays a significant role as regards the \mathcal{S} factor of Eq. (7) as well as the annihilation volume ξ through the dependence of the maximum density in the core, given by Eq. (19).

In the framework of the Minimal Supersymmetric Standard Model (MSSM) with a gravity driven supersymmetry breaking (mSUGRA), we choose two specific sets of parameters leading to two typical DM candidates.

The latter are a *bino* and a *Higgsino* (respectively referred to as \tilde{B} and \tilde{H} in the following), depending on the field content of the lightest supersymmetric particle. They differ mainly in their couplings to the Standard Model particles and thus have different annihilation final states. The public code SuSpect [66] is used to derive the weak-scale parameters from the mSUGRA inputs by solving the renormalization group equations. The cross sections for the different final states have been determined with the micrOMEGAS [68, 69] package.

The first Kaluza-Klein model considers warped extra-dimensions with a SO(10) GUT, as described in [70]. In that context the DM particle is a right handed Dirac neutrino. Its stability arises from the conservation of a \mathbf{Z}_3 symmetry – hence its name LZP for Lightest Z Particle. To fulfill the relic density constraints, we choose $M_{KK} = 6$ TeV and $m_{LZP} = 50$ GeV respectively for the Kaluza-Klein scale and the LZP mass. The second Kaluza-Klein model assumes universal extra-dimensions with $R^{-1} = 1$ TeV [71]. Then, the DM particle is the lightest particle with odd K-parity, which happens to be the first Kaluza-Klein excitation of the B^0 hypercharge gauge boson, referred to as the $B^{(1)}$ (or LKP) with mass $m_{LKP} = 1$ TeV.

All the relevant particle physics parameters and the inferred values regarding the maximum density and the mean annihilation volume $\langle \xi \rangle$ are summarized in Tab. I. Monte Carlo simulations are performed in the context of these four models. The LZP being a Dirac particle, one has $\delta = 1/4$ in that case, whereas $\delta = 1/2$ otherwise. The results are presented in Fig. 8 for positrons and in Fig. 9 for antiprotons. The absolute fluxes are featured together with the actual data points. The positron flux measurements are taken from HEAT- e^\pm [72] and HEAT-pbar experiments [73] and two independent analyses of AMS01 data [74, 75]. For antiprotons, we borrowed the results from [77, 78, 79, 80].

We first discuss the positron case. In Fig. 8, the dashed line is the unboosted, and therefore guaranteed, exotic flux in the framework of the considered models. In each case, the yellow (grey) area represents the flux uncertainty with IMBH mini-spikes. For clarity, the bright yellow contours stand for the $\sigma/2$ level whereas the 1σ contours are indicated by the pale yellow regions. In the four models we have considered, the positron flux at 10 GeV is in the range between $\sim 6 \times 10^{-6}$ and $\sim 3 \times 10^{-5}$ cm⁻² s⁻¹ GeV⁻¹ sr⁻¹. The exotic fluxes generated by IMBH mini-spikes are fairly insensitive to the annihilation cross section, as a consequence of Eq. (22). We unexpectedly find that the flux is not very sensitive to the mass. This is because the injection spectrum $g(E_S)$ softens the $m_\chi^{-9/7}$ dependence of the annihilation rate inferred from that relation. In addition, the variance of the flux is significantly smaller in the LKP case. Indeed, the injection spectrum $g(E_S)$ extends up to 1 TeV and has an important high energy contribution. As a consequence, the sensitivity sphere below ~ 10 GeV has a wider spread than for the three other DM candidates. The LKP flux

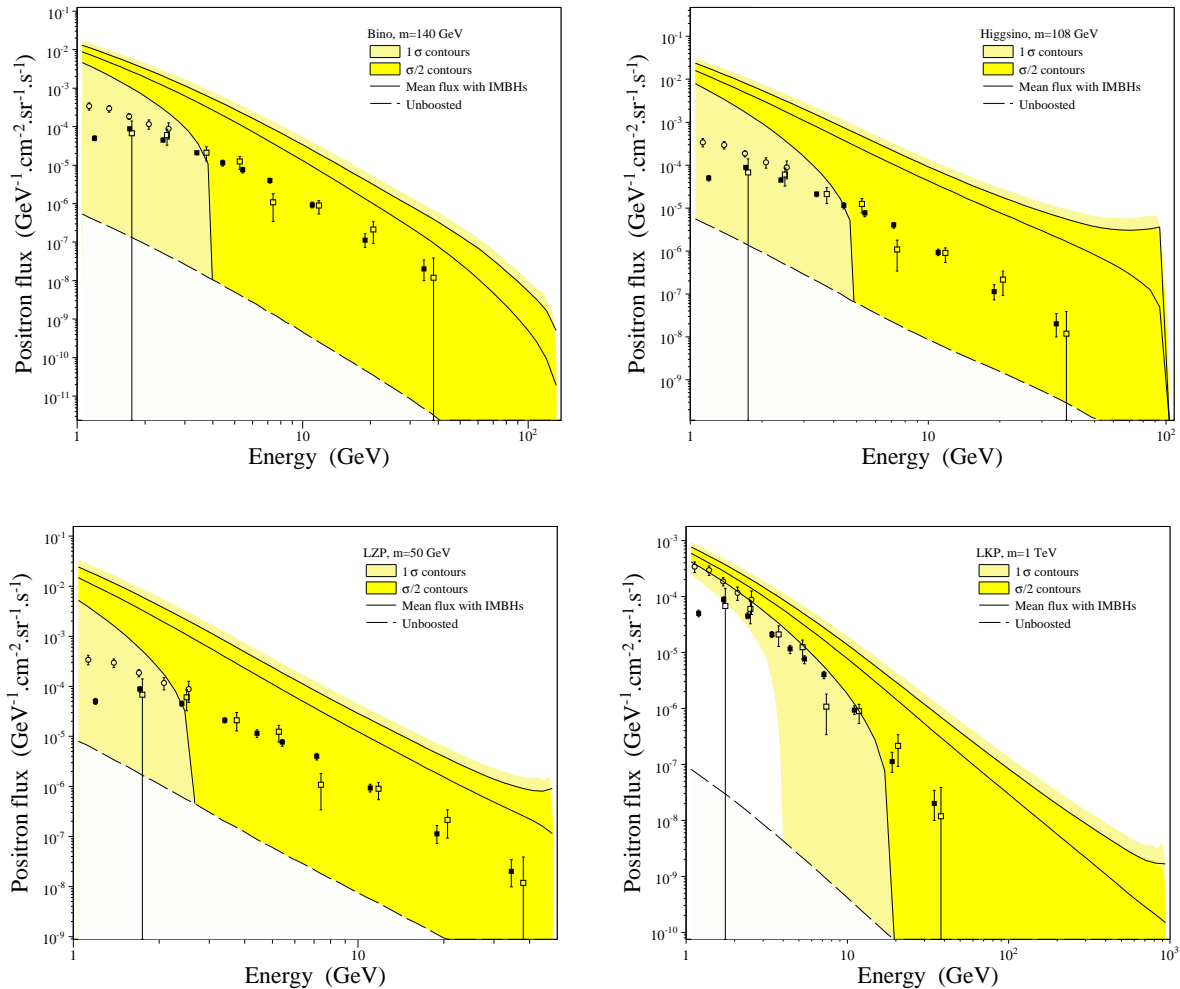


FIG. 8: Exotic positron fluxes in four particle physics models (top : supersymmetric DM, bottom : Kaluza-Klein DM) within IMBHs mini-spike scenario, and comparison to actual measurements. The bright and the pale yellow areas respectively correspond to contours at the $\sigma/2$ and 1σ level.

is less sensitive to the shotnoise associated with the random realization of the IMBH population. The other cases feature a higher dispersion, mainly due to the fact that the DM particle mass is lower and the sensitivity sphere smaller.

We now discuss the antiproton case. The results are displayed in Fig. 9, along with the standard flux, for the same set of propagation parameters as for the positrons (see Sec. III). In the case of a smooth halo, the exotic contribution is always lower than the flux due to standard processes. When IMBH mini-spikes are considered, the antiproton flux at 10 GeV is in the range between $\sim 3 \times 10^{-2}$ and $\sim 4 \times 10^{-1} \text{ m}^{-2} \text{ s}^{-1} \text{ GeV}^{-1} \text{ sr}^{-1}$ in the four models we have considered. We observe the same delicate interplay between the mass dependence of the annihilation rate and the energy behaviour of the injection spectrum $g(E_S)$ – though the later is less dependent on

the final state species than for positrons. As before, the antiproton flux is weakly dependent on the annihilation cross section. This is particularly obvious in the two upper panels, between which $\langle \sigma_{\text{ann}} v \rangle$ varies by a factor ~ 7 . Below ~ 20 GeV, the antiproton primary fluxes have a very large scatter, as explained in Sec. IV C.

VI. DISCUSSION AND PERSPECTIVES

We have considered a scenario in which the formation of IMBHs generates dramatic enhancements of the DM density in their vicinity. We have computed the expected number of unmerged IMBHs in the Galactic halo, their spatial distribution and the properties of their associated mini-spikes. We found high values for the positron and antiproton boost factors, e.g. of order 10^4 for a fiducial

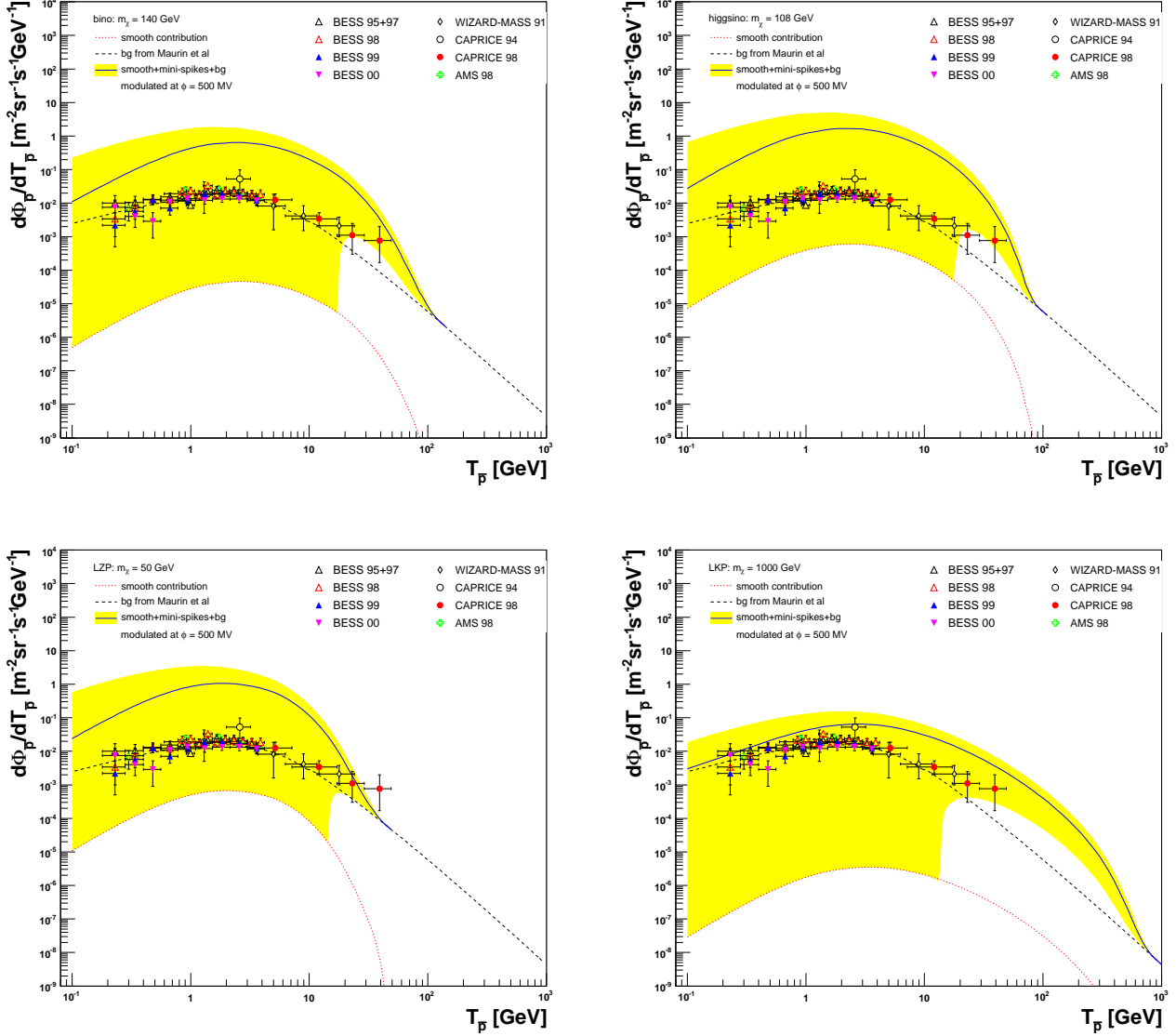


FIG. 9: Antiproton fluxes as a function of kinetic energy in the case of a bino dark matter particle with mass $m_\chi = 140$ GeV. The fluxes were computed without (upper panel) or with (lower panel) wind (with a value $V_c = 12$ km/s), without (left) or with (right) spallation.

DM particle with a 1 TeV mass. For an average mini-spike population, the flux of primary positrons and antiprotons turns out to be one to two orders of magnitude larger than the measured flux, and is fairly insensitive to the specific properties of the DM candidate. In particular, the annihilation cross section has little influence because of the presence of an annihilation plateau in the cores of mini-spikes. This interesting feature allows configurations in the particle physics parameter space which are usually disregarded – because of their very low cross sections – to become testable. As the average flux signal exceeds the data points, we could naively conclude that the mini-spike scenario is already ruled out by observation. However, because of the small number of objects,

the variance associated to the positron and antiproton signal is enormous and no definitive conclusion can be reached. We leave for further investigation the quantitative estimate of the confidence level at which the mini-spike scenario agrees with measurements.

Notice finally that this variance is small at low energy for positrons, and on the contrary at high energy for antiprotons. Should a cut-off above some specific energy E_c be detected in the positron flux, the natural interpretation would lead to a DM particle mass $m_\chi \sim E_c$. The possible existence of substructures leaves room to more subtle explanations. In particular, if an excess in the antiproton flux were found above E_c , we would conclude that we live in a particular Milky Way realization where

substructures are far from the Earth. The farther those substructures, the smaller E_c with respect to m_χ , hence the possibility of a misinterpretation of the data. This illustrates the fact that combining various indirect signals could give information about the spatial distribution of DM.

Acknowledgments

We thank Andrew Zentner for early collaboration and for making available the numerical realizations of IMBHs

in the Milky Way, on which our calculations are based. We thank the French Programme National de Cosmologie (PNC) for its financial support. P.B. wishes to thank Stéphane Ranchon and the H.E.S.S. team of LAPP for providing help and CPU for this project. G.B. acknowledges the support, during the first part of this project, by the Helmholtz Association of National Research Centres. J.L. is grateful to the French GDR SUSY and the CPPM-ANTARES group for having supported this work. We also thank D. Hooper for valuable comments.

-
- [1] L. Bergstrom, Rept. Prog. Phys. **63** (2000) 793 [arXiv:hep-ph/0002126].
- [2] C. Munoz, Int. J. Mod. Phys. A **19**, 3093 (2004) [arXiv:hep-ph/0309346].
- [3] G. Bertone, D. Hooper and J. Silk, Phys. Rept. **405** (2005) 279 [arXiv:hep-ph/0404175].
- [4] <http://www-glast.stanford.edu/>
- [5] <http://icrhp9.icrr.u-tokyo.ac.jp/index.html>
- [6] <http://www.mpi-hd.mpg.de/hfm/HESS/HESS.html>
- [7] <http://hegra1.mppmu.mpg.de/MAGICWeb/>
- [8] <http://veritas.sao.arizona.edu/index.html>
- [9] J. Ahrens *et al.* [The IceCube Collaboration], Nucl. Phys. Proc. Suppl. **118**, 388 (2003) [arXiv:astro-ph/0209556].
- [10] E. Aslanides *et al.* [ANTARES Collaboration], arXiv:astro-ph/9907432.
- [11] G. L. Kane, L. T. Wang and J. D. Wells, Phys. Rev. D **65**, 057701 (2002).
- [12] M. Kamionkowski and M. S. Turner, Phys. Rev. D **43**, 1774 (1991).
- [13] M. S. Turner and F. Wilczek, Phys. Rev. D, **42**, 1001 (1990).
- [14] A. J. Tylka, Phys. Rev. Lett., **63**, 840 (1989).
- [15] G. L. Kane, L. T. Wang and T. T. Wang, Phys. Lett. B **536**, 263 (2002).
- [16] E. A. Baltz and J. Edsjo, Phys. Rev. D **59** (1999) 023511 [arXiv:astro-ph/9808243].
- [17] E. A. Baltz, J. Edsjo, K. Freese and P. Gondolo, Phys. Rev. D **65** (2002) 063511 [arXiv:astro-ph/0109318].
- [18] H. C. Cheng, J. L. Feng and K. T. Matchev, Phys. Rev. Lett. **89**, 211301 (2002) [arXiv:hep-ph/0207125].
- [19] J. Lavalle, J. Pochon, P. Salati and R. Taillet, Astron. Astrophys. **462**, 827 (2007) [arXiv:astro-ph/0603796].
- [20] A. Bottino, F. Donato, N. Fornengo and P. Salati, Phys. Rev. D **58**, 123503 (1998).
- [21] F. Donato, N. Fornengo, D. Maurin, P. Salati and R. Taillet, Phys. Rev. D **69**, 063501 (2004) [arXiv:astro-ph/0306207].
- [22] L. Bergstrom, J. Edsjo and P. Ullio, ApJ **526**, 215 (1999) [arXiv:astro-ph/9902012].
- [23] A.M. Lionetto, A. Morselli, V. Zdravkovic, JCAP **09**, 010 (2005) [astro-ph/0502406]
- [24] P. Picozza *et al.*, arXiv:astro-ph/0608697.
- [25] <http://ams.cern.ch/>
- [26] G. Bertone, Phys. Rev. D **73** (2006) 103519 [arXiv:astro-ph/0603148].
- [27] M. C. Miller and E. J. M. Colbert, Int. J. Mod. Phys. D **13** (2004) 1 [arXiv:astro-ph/0308402].
- [28] Fryer, C. L., & Kalogera, V. 2001, Astrophys. J. 554, 548
- [29] R. Narayan, arXiv:astro-ph/0310692.
- [30] Ferrarese, L., & Ford, H. 2005, Space Science Reviews, 116, 523
- [31] Kormendy, J., & Richstone, D. 1995, Ann. Rev. Astron. & Astrophys., 33, 581
- [32] L. Ferrarese and D. Merritt, Astrophys. J. **539** (2000) L9 [arXiv:astro-ph/0006053].
- [33] R. J. McLure and J. S. Dunlop, Mon. Not. Roy. Astron. Soc. **331** (2002) 795 [arXiv:astro-ph/0108417].
- [34] K. Gebhardt *et al.*, Astrophys. J. **539** (2000) L13 [arXiv:astro-ph/0006289].
- [35] S. Tremaine *et al.*, Astrophys. J. **574** (2002) 740 [arXiv:astro-ph/0203468].
- [36] X. Fan *et al.* [SDSS Collaboration], Astron. J. **122** (2001) 2833 [arXiv:astro-ph/0108063].
- [37] Barth, A. J., Martini, P., Nelson, C. H., & Ho, L. C. 2003, Astrophys. Lett. 594, L95.
- [38] C. J. Willott, R. J. McLure and M. J. Jarvis, Astrophys. J. **587** (2003) L15 [arXiv:astro-ph/0303062].
- [39] Haiman, Z., & Loeb, A. 2001, Astrophys. J. , 552, 459.
- [40] G. Bertone, A. R. Zentner and J. Silk, Phys. Rev. D **72** (2005) 103517 [arXiv:astro-ph/0509565].
- [41] Madau, P., & Rees, M. J. 2001, Astrophys. J. Lett. 551, L27.
- [42] H. S. Zhao and J. Silk, arXiv:astro-ph/0501625.
- [43] R. Islam, J. Taylor and J. Silk, Mon. Not. Roy. Astron. Soc. **354** (2003) 443.
- [44] R. Islam, J. Taylor and J. Silk, Mon. Not. Roy. Astron. Soc. **354** (2004) 427.
- [45] S. M. Koushiappas, J. S. Bullock and A. Dekel, Mon. Not. Roy. Astron. Soc. **354** (2004) 292 [arXiv:astro-ph/0311487].
- [46] Peebles, P. J. E. 1972, Astrophys. J. 178, 371.
- [47] P. Young, 1980, Astrophys. J. **242** (1980), 1232.
- [48] J. R. Ipser and P. Sikivie, Phys. Rev. D **35** (1987) 3695.
- [49] Quinlan, G. D., Hernquist, L., & Sigurdsson, S. 1995, Astrophys. J. **440**, 554.
- [50] P. Gondolo and J. Silk, Phys. Rev. Lett. **83** (1999) 1719, [arXiv:astro-ph/9906391].
- [51] D. Merritt, Proceedings of Carnegie Observatories Centennial Symposium *Coevolution of Black Holes and Galaxies* [arXiv:astro-ph/0301257].

- [52] G. Bertone and D. Merritt, *Mod. Phys. Lett. A* **20** (2005) 1021 [arXiv:astro-ph/0504422].
- [53] G. Bertone and D. Merritt, *Phys. Rev. D* **72** (2005) 103502 [arXiv:astro-ph/0501555].
- [54] P. Ullio, H. Zhao and M. Kamionkowski, *Phys. Rev. D* **64**, 043504 (2001) [arXiv:astro-ph/0101481].
- [55] D. Merritt, M. Milosavljevic, L. Verde and R. Jimenez, arXiv:astro-ph/0201376.
- [56] D. Merritt, arXiv:astro-ph/0301365.
- [57] D. Merritt, S. Harfst and G. Bertone, arXiv:astro-ph/0610425.
- [58] J. F. Navarro, C. S. Frenk and S. D. M. White, *Astrophys. J.* **490**, (1997) 493.
- [59] J. F. Navarro *et al.*, *Mon. Not. R. Astron. Soc.* **349**, 1039 (2004).
- [60] D. Reed *et al.*, *Mon. Not. R. Astron. Soc.* **357**, 82 (2005).
- [61] D. Merritt, J. Navarro, A. Ludlow, and A. Jenkins, astro-ph/0502515 (2005).
- [62] S. M. Koushiappas and A. R. Zentner, *Astrophys. J.* **639**, (2006) 7.
- [63] T. Appelquist, H. C. Cheng and B. A. Dobrescu, *Phys. Rev. D* **64**, (2001) 035002.
- [64] D. Maurin, R. Taillet and C. Combet, [arXiv:astro-ph/0609522].
- [65] T. Bringmann and P. Salati, [arXiv:astro-ph/0612514].
- [66] A. Djouadi, J.L. Kneur, G. Mourtaka, G., 2002, [arXiv:hep-ph/0211331]
<http://www.lpta.univ-montp2.fr/~kneur/Suspect>
- [67] T. Sjöstrand, S. Mrenna, Peter Skands, 2006, *JHEP*, **0605**, 026 [arXiv:hep-ph/0603175]
- [68] G. Bélanger, F. Boudjema, A. Pukhov, A. Semenov, 2002, *Comput. Phys. Commun.*, **149**, 103 [arXiv: hep-ph/0112278]
- [69] G. Bélanger, F. Boudjema, A. Pukhov, A. Semenov, 2006, *Comput. Phys. Commun.*, **174**, 577 [arXiv: hep-ph/0405253]
- [70] K. Agashe, G. Servant, 2004, *Phys. Rev. Lett.*, **93**, 231805 [arXiv: hep-ph/0403143]
- [71] G. Servant, T. Tait, 2003, *Nucl. Phys.*, B, **650**, 391 [arXiv: hep-ph/0206071]
- [72] S. Coutu *et al.*, 1999, *Astropart. Phys.*, **11**, 429 [arXiv: astro-ph/9902162]
- [73] J.J. Beatty *et al.*, 2004, *Phys. Rev. Lett.*, **93**, 241102 [arXiv: astro-ph/0412230]
- [74] [AMS Collaboration] J. Alcaraz *et al.*, 2000, *Phys. Lett.*, B, **484**, 10
- [75] [AMS Collaboration] M. Aguilar *et al.*, 2007, *Phys. Lett.*, B, **646**, 145 [arXiv: astro-ph/0605254]
- [76] F. Donato, N. Fornengo, D. Maurin, P. Salati and R. Taillet, D. Maurin, R. Taillet, F. Donato, P. Salati, A. Barrau and G. Boudoul [arXiv:astro-ph/0212111]
- [77] S. Orito *et al.* [BESS Collaboration], *Phys. Rev. Lett.* **84**, 1078 (2000) [arXiv:astro-ph/9906426].
- [78] T. Maeno *et al.* [BESS Collaboration], positive Astropart. Phys. **16**, 121 (2001) [arXiv:astro-ph/0010381].
- [79] M. Boezio *et al.* [WiZard/CAPRICE Collaboration], *Astrophys. J.* **561**, 787 (2001) [arXiv:astro-ph/0103513].
- [80] M. Aguilar *et al.* [AMS Collaboration], Space Station. I: *Phys. Rep.* **366**, 331 (2002), Erratum-ibid. **380**, 97 (2003).

	\tilde{B}	\tilde{H}	LZP	LKP
m	140 GeV	108 GeV	50 GeV	1 TeV
$\sigma v (\times 10^{-26} \text{ cm}^3 \text{ s}^{-1})$	0.26	1.9	2.04	1.7
Final States	$b\bar{b}$ 91% $\tau^+\tau^-$ 9%	W^+W^- 90% Z^0Z^0 10%	$q\bar{q}$ 74% $\nu\bar{\nu}$ 17% $\ell^+\ell^-$ 2.88% ($\times 3$)	$q\bar{q}_{up}$ 11% ($\times 3$) $q\bar{q}_{down}$ 1% ($\times 3$) $\nu\bar{\nu}$ 4% $\ell^+\ell^-$ 20% ($\times 3$)
$\rho_{\text{max}} (\times 10^{17} \text{ M}_{\odot} \text{ kpc}^{-3})$	47.1	4.97	2.15	51.5
$\langle \xi \rangle (\times 10^5 \text{ kpc}^3)$	46.6	9.35	5.14	49.6

TABLE I: Relevant parameters for the particle dark matter models discussed in Sec. V.